RSC Advances

PAPER

View Article Online
View Journal | View Issue

Cite this: *RSC Adv.*, 2020, **10**, 18753

Anomalous transport and magnetic properties induced by slight Cu valence alternation in layered oxytelluride BiCuTeO

Ye-Cheng Luo,[a] Dajun Lin,[b] Yan-Yan Zhang,[b] Song-Tao Dong,[c] Shu-Hua Yao,[b] Yang-Yang Lv,*[a] Jian Zhou[b] and Y. B. Chen*[ad]

Received 26th March 2020
Accepted 10th May 2020

DOI: 10.1039/d0ra02763d

rsc.li/rsc-advances

In this paper, we report on the transport and magnetic properties of layered oxytelluride BiCuTeO polycrystals with slight mixed valence of Cu. The temperature-dependent electrical resistivity reveals degenerate semiconductor behavior (similar to metals). Under the action of an external magnetic field, the BiCuTeO polycrystal sample exhibits unsaturated magnetic resistance (MR) of about 8% at 2 K and 9 Tesla. The Hall resistivities show nonlinear behavior, suggesting the coexistence of both electrons and holes in the sample. When the temperature is decreased to around 110 K, the dominant carriers are changed from electrons to holes from the viewpoint of electrical transport, which is supported by the calculated temperature-dependent Fermi energy. Meanwhile, at low temperatures (<100 K), the impurity magnetic moment formed by a small amount of positive divalent copper exhibits short-range magnetism (a spin-glass-like feature), which gives rise to a narrow magnetic hysteresis loop. Our work may benefit in-depth understanding of physical properties of BiCuTeO-based materials.

1. Introduction

Over the past few decades, quaternary compounds with a general formula MNXO (M = trivalent cation; N = Ag, Fe, Cu, *etc.*; X = pnictogen or chalcogen) have prompted a great deal of research.[1–4] These materials crystallize in the same tetragonal ZrCuSiAs structure type with the *P*4/*nmm* space group,[2] comprising $(N_2X_2)^{2-}$ layers alternately stacked with $(M_2O_2)^{2+}$ layers along the *c*-axis by weak ionic bonds, where the former transfer carriers and the latter reserve carriers. With such a two-dimensional (2D) layered structure, they have been established with distinct element combinations exhibiting rich physical properties and potential application prospects, such as superconductivity in 1111 iron-based materials,[5–8] and good optoelectronic and thermoelectric performance in 1111 copper-based materials.[9–12]

Among these quaternary compounds, a promising thermoelectric (TE) material BiCuSeO has attracted intensive research interest in recent years.[11–13] The thermoelectric figure of merit (ZT) is defined as $ZT = S^2T\sigma/\lambda$, where S, σ, T, λ and are the Seebeck coefficient, electrical conductivity, absolute temperature, and thermal conductivity respectively. Due to the large Seebeck coefficient (>300 μV K^{-1}) and low thermal conductivity (~0.2 W m^{-1} K^{-1} at high temperature), the ZT value of BiCuSeO can reach up to ~1.5 after many attempts for optimizing thermoelectric properties, which exhibits a favorable potential for thermoelectric devices.[14–17]

As a rational chemical approach, introduction of Cu vacancies could effectively enhance the electrical conductivity so as to improve thermoelectric performance of BiCuSeO.[18,19] In addition, the Cu defect also bring about some unique physical properties in BiCuSeO-based materials. For example, a large magnetoresistance, ferromagnetic and antiferromagnetic coupling, and charge transfer between the conduction and magnetic electrons caused by Cu vacancies were observed in $BiCu_{0.96}SeO$.[20] The similar spin-charge couplings were also found in Cu-deficient $BiCu_{0.94}SO$.[21] Of particular concern is, theoretical studies suggested BiCuSO would exhibit superconductivity with appropriate doping.[22] And then, the superconductivity was found in $BiOCu_{1-x}S$ as reported by Ubaldini *et al.*[23] The new superconducting compound having similar structure of the Fe oxypnictide superconductors,[4] which provides a useful clue to look for more layered 1111 structure superconducting compounds.[24] Based on the above, it is believed that Cu deficiency plays a key role in exploring new physical properties in this class of materials (BiCuSO, BiCuSeO and BiCuTeO).

In our previous report,[25] we have studied electrical and magneto-transport properties of BiCuTeO polycrystal with

[a]*National Laboratory of Solid State Microstructures, Department of Physics, Nanjing University, Nanjing 210093, China. E-mail: lvyangws0801@nju.edu.cn; ybchen@nju.edu.cn*

[b]*National Laboratory of Solid State Microstructures, Jiangsu Key Laboratory of Artificial Functional Materials, Department of Materials Science and Engineering, Nanjing University, Nanjing 210093, China*

[c]*Institute of Materials Science and Engineering, Jiangsu University of Science and Technology, Zhenjiang 212003, China*

[d]*Collaborative Innovation Center of Advanced Microstructure, Nanjing University, Nanjing, 210093, China*

slight Bi vacancies. Here, we introduced slight Cu mixed-valence in BiCuTeO by adjusting growth parameters to observe its possibly novel physical properties. Systematic structure, component, transport and magnetic properties of the as-prepared samples were investigated. Particularly, these bulk BiCuTeO materials exhibit a metal type behavior, an unsaturated magnetoresistance (MR) and nonlinear Hall resistivities caused by the coexistence of both electron and hole. At low temperatures, the magnetic moment of impurities formed by a small amount of divalent Cu shows the short-range magnetism. Meanwhile the diamagnetic contributed by the coexistence of two carriers appears at high temperature (~90 K).

2. Experiments

2.1 Synthesis of BiCuTeO polycrystals

BiCuTeO powder has been synthesized by a direct solid-state reaction with highly pure Bi (Alfa Aesar 99.999%), Bi_2O_3 (Sinopharm Chemical Reagent 99.99%), Cu (Sinopharm Chemical Reagent 99.99%), and Te (Alfa Aesar 99.999%) powders using high purity quartz ampoules as the reactor.[18] The mixtures were placed in the sealed and evacuated quartz ampoules, heated to 300 °C at a rate of 100 °C h^{-1} and held at this temperature for 20 h. And then the container were heated to 580 °C in 3 h and kept at this temperature for 72 h until the reaction completed. *It should be emphasized that in this work, the raw powder of Bi–Bi_2O_3–Cu–Te was heated to 580 °C in 3 h and kept at this temperature for 72 h until the reaction completed; but in our previous work,[25] these raw powders were heated to 550 °C in 2 h and kept at this temperature for 48 h.* The obtained bulk products were crushed and finely grinded into powders. Then the powders were hot-pressed into a disk-shaped sample (pellet) of ϕ 10 mm × 2.5 mm under the axial compressive stress of 15 MPa. Finally, the as-prepared pellet samples were heated again at 550 °C (held about 6 h) to obtain bulk BiCuTeO material. The final BiCuTeO samples were cut into the flake with the size of about 3 mm × 2 mm × 1 mm for experimental measurement. All sample preparation processes, including the weighing of raw materials and grinding of powders, were carried out in air.

2.2 Characterization

Room temperature X-ray diffraction (XRD) was carried on Ultima III Rigaku X-ray diffractometer, Cu-K_α radiation with 2θ scanned from 5° to 60° was applied to investigate crystal structure of samples. The elemental compositions of the samples were determined by an energy dispersive spectrometer (EDS) equipped in a scanning electron microscope (SEM) (FEI-Quanta) with the internal calibration. The accelerating voltage for the SEM in the experiment is 25 kV. Standard six-probe method was employed on the roughly rectangular crystals for the electrical transport measurements which were performed in a 9 T physical properties measurement system (PPMS, Quantum Design). During the electrical measurement, platinum wire was used as electrodes. Magnetic tests were carried out in superconductor quantum interference device (SQUID, Quantum Design). X-ray photoelectron spectrum (XPS) was used for detecting element binding energy and valence analysis.

3. Results and discussion

3.1 Crystal diffraction and composition of elements

Room temperature X-ray diffraction characterization was performed with 2θ scanned from 5° to 60° (as shown in Fig. 1(a)). The specific peak position marks the calculated facet index.[25] It should be mentioned that we have not found any reflections coming from CuO impurity phase from XRD data. Fig. 1(b) shows the EDS results of Bi, Cu, O, and Te elements in bulk BiCuTeO polycrystal sample. Quantitative EDS analysis indicates that the ratio among Bi, Cu, O, and Te is 1 : 0.93 : 1.05 : 0.96, which is close to the stoichiometric formula. In addition, the compounds should keep electrical neutrality; therefore the ratio of Cu^{2+} impurity in Cu elements can be determined as 9.7% by means of EDS data.

The valence of each element and element category is judged by the X-ray photoelectron spectroscopy to reflect the binding energy of the elements.[26] The high resolution patterns are presented in Fig. 2. The characteristic peak of the Bi element in Fig. 2(a) appears at 158.5 eV and 163.8 eV, a gap between the Bi $4f_{7/2}$ and Bi $4f_{5/2}$ peaks of 5.3 eV, which represents the Bi^{3+} oxidation state of this element. However, the Cu $2p_{1/2}$ and $2p_{3/2}$

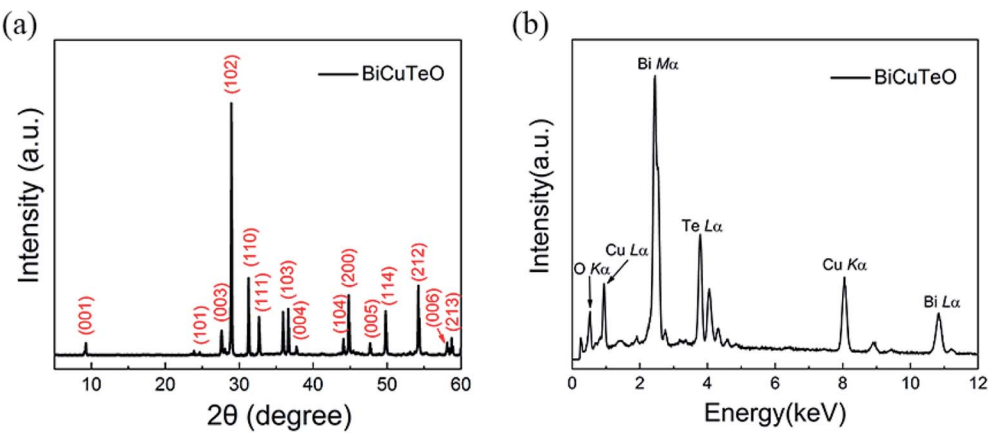

Fig. 1 (a) Room temperature XRD pattern of the representative BiCuTeO poly-crystals measured in *ab* plane. (b) The EDS spectra of selective BiCuTeO sample. The major characteristic X-ray peaks of Bi, Cu, Te and O are labeled in the spectra, respectively.

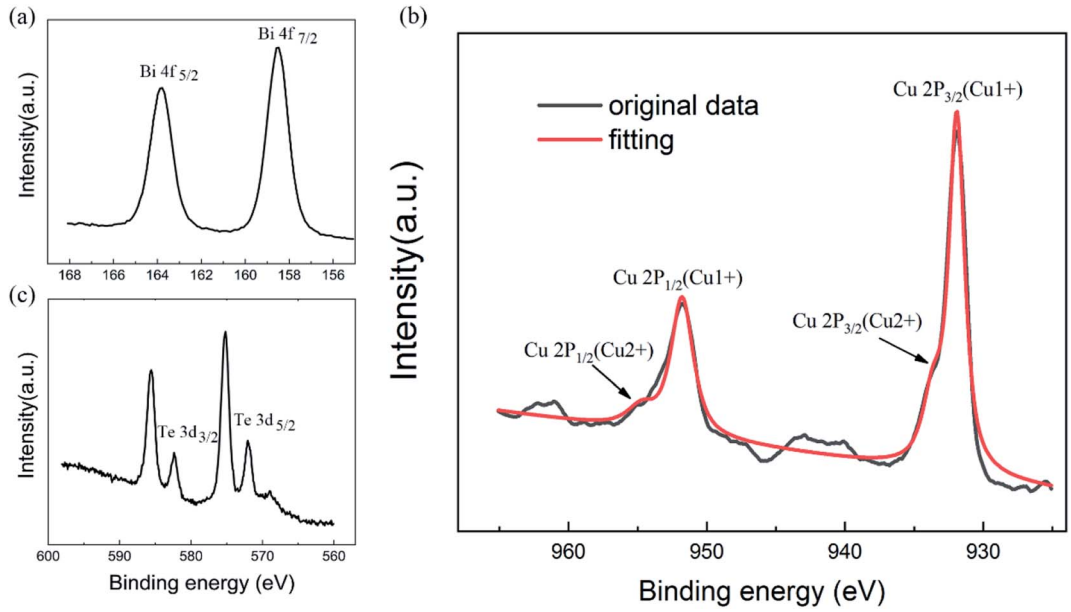

Fig. 2 X-ray photoelectron spectroscopy of selective BiCuTeO sample. (a), (b) and (c) represents Bi, Cu and Te elements, respectively. The spectrum of Cu shows the co-existence of Cu^{1+} and Cu^{2+} ions, the fitting line was marked as red color.

peaks in BiCuTeO (see Fig. 2(b)) verify that this element is mainly at the +1 oxidation state, with a gap of 20 eV between these two main peaks. Cu^{2+} species are also observed on this spectrum, characterized by shoulders on the Cu^{+} peaks at 933.8 eV and 954.9 eV. Quantitively, by fitting results (see red color line in Fig. 2(b)) with XPS peaks software, the amount of

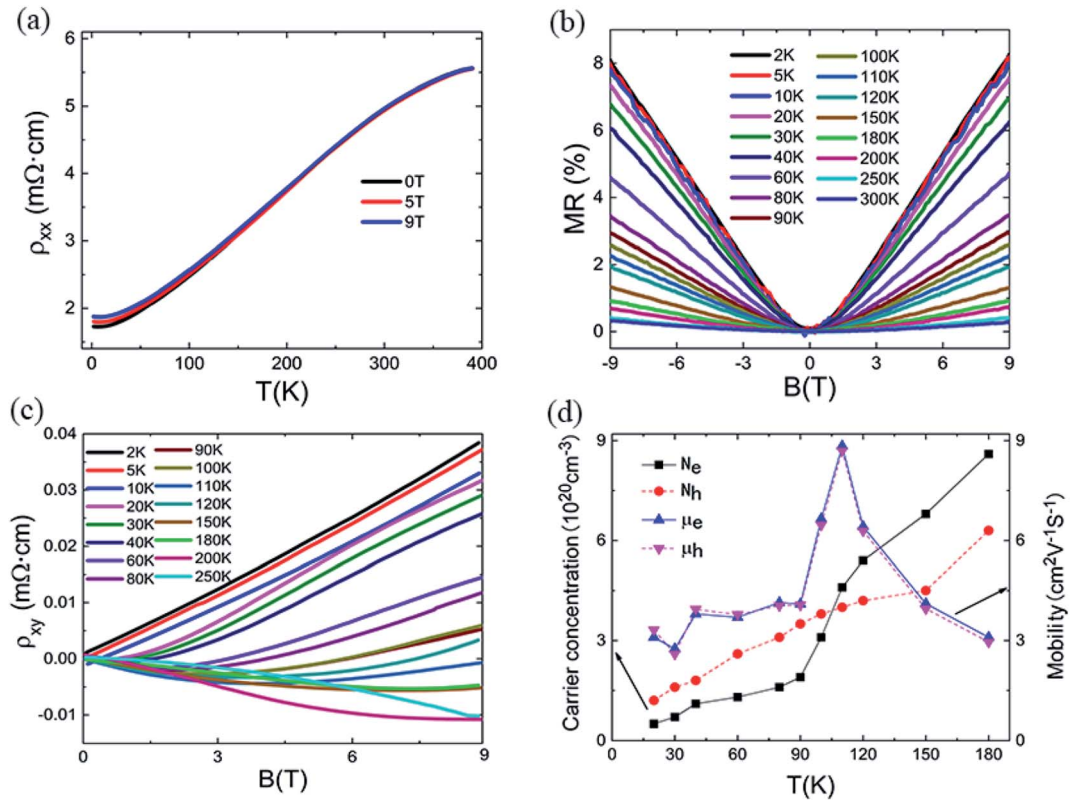

Fig. 3 (a) Temperature dependent resistivity ratio under different applied magnetic field of 0 T, 5 T and 9 T. (b) Magnetic field dependent magnetic resistivity for series fixed temperature points. (c) The *B* related Hall resistivity of sample under temperature range from 2 K to 250 K. (d) Carrier concentrations and motilities for electron and hole fitted with two-band model.

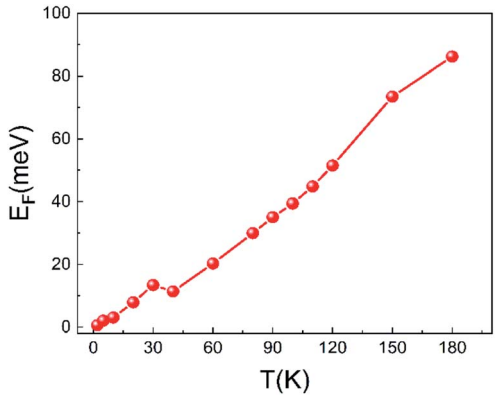

Fig. 4 Temperature dependent Fermi energy variety of BiCuTeO from theory calculation.

Cu^{2+} impurity takes up 11.2% in all Cu elements by calculating the ratio of peaks area. This result is consistent to EDS data. Considering the finite errors in EDS characterization and XPS fitting, the probability of Cu^{2+} ratio is around 10.0%. Therefore, it can be elementally judged that the Cu element in the BiCuTeO sample is mainly +1 valence. Fig. 2(c) shows the binding energies of Te elements. The corresponding valence state is −2 with diagnostic peaks at 573.1 eV and 583.2 eV labeled as Te $3d_{5/2}$ and Te $3d_{3/2}$, respectively.

3.2 Analysis of electron charge transport

Fig. 3(a) shows the temperature dependence of resistivity ρ_{xx} measured under various external magnetic field B perpendicular to electric field I. Under zero field, ρ_{xx} exhibits a metallic behavior. Quantitatively, ρ_{xx} are 1.73 mΩ cm and 5.56 mΩ cm at 2 K and 390 K, respectively. The residual resistivity ratio (RRR) of the sample was calculated as 3.21. With application of 5 Tesla and 9 Tesla magnetic field, the sample still shows a metallic behavior. Due to the Lorentz cyclotron motion caused by B, the scattering of electrons is increased, which is not reflected in the high temperature range. In the low temperature region, the residual resistance increases as the B increases. Fig. 3(b) shows the field-dependence of magnetoresistance (MR) of bulk BiCuTeO sample at different temperature. The MR is defined as $MR = [R_{xx}(B) - R_{xx}(0)]/R_{xx}(0) \times 100\%$, where $R_{xx}(0)$ and $R_{xx}(B)$ are the resistance measured at zero magnetic field and an applied magnetic field B, respectively. At 2 K, the magnetoresistance is 8% under 9 T, indicating that the influence of the magnetic field on the electron scattering is too slight, which is consistent with the performance of the temperature dependence of resistivity ρ_{xx} in the low temperature region measured under various external magnetic field (see Fig. 3(a)). The Hall data are depicted in Fig. 3(c). One can see, at 2 K, 5 K, and 10 K, the Hall resistivity increases linearly with the augment of the external magnetic field, and the carriers in the sample are holes. When the temperature is higher than 20 K, electron carriers begin to appear. This is because a few electrons are in the Cu defect level at low temperature. Electrons hop from the defect level to the conduction band by thermal excitation, and then participate in the transport process. In addition, up to 100 K, holes are the dominant carriers. Electron become the dominant carriers until temperature above 110 K. Fig. 3(d) shows the temperature-dependent carrier concentrations and mobilities which were calculated by means of two-band model (eqn (1)),

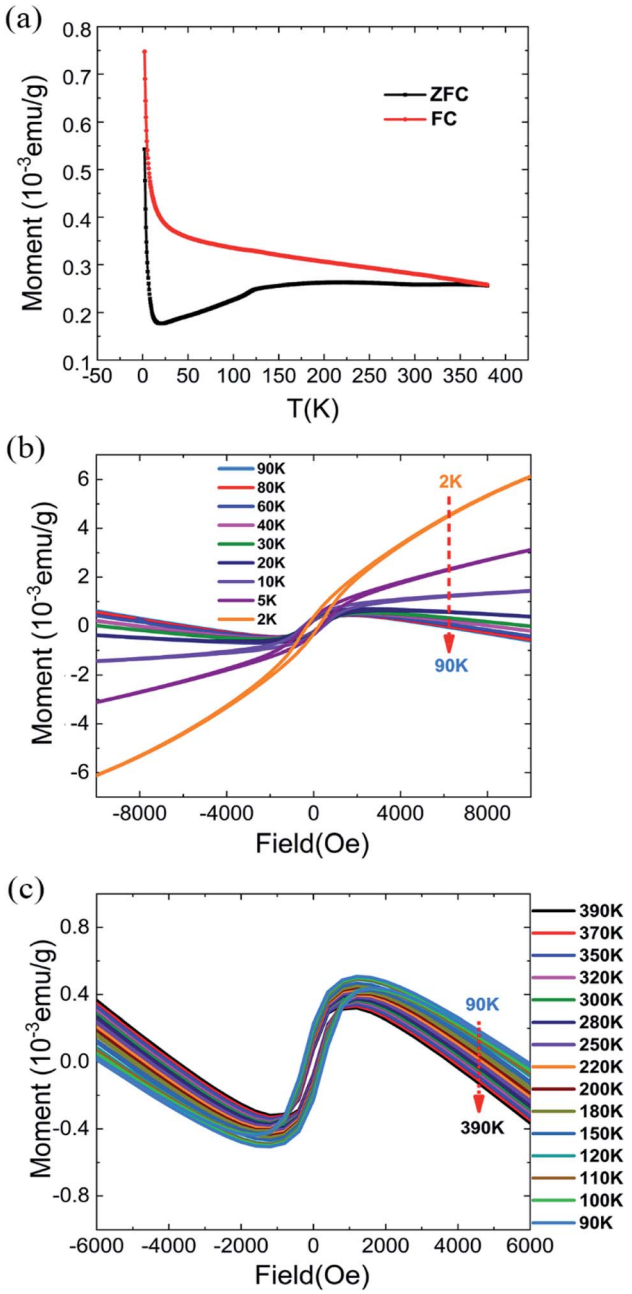

Fig. 5 (a) Magnetization vary with temperature under external magnetic field cooling and zero magnetic field cooling. (b) and (c) Magnetization loops of BiCuTeO taken from 2 K to 390 K. Magnetic hysteresis appears in low field (about 4000 Oe) of loops collected at 2 K, 5 K and 10 K.

$$\rho_{xy} = \frac{B}{e}\frac{(n_h\mu_h^2 - n_e\mu_e^2) + (n_h - n_e)\mu_h^2\mu_e^2B^2}{(n_h\mu_h + n_e\mu_e)^2 + (n_h - n_e)^2\mu_h^2\mu_e^2B^2} \quad (1)$$

where n_e is the electron concentration, n_h is the hole concentration, μ_e is the electron mobility, and μ_h is the hole mobility.[27] Under the assumption that μ_e is approximate with μ_h and consider the absolute value $|n_e - n_h|$ as a small amount to $n_e + n_h$. Then hall resistivity can be expressed as $\rho_{xy} = a \times B + b \times B^2 + c \times B^3$. The above four parameters are obtained by these conditions. With the temperature increasing, the electron and hole carrier concentrations heighten simultaneously, and the carrier concentration is on the order of 10^{20} cm^{-3}. The mobility of electrons and holes has a peak of 8.6 cm^2 V^{-1} S^{-1} at 110 K, which is due to the close carrier concentration. Meanwhile, the BiCuTeO band gap acquired from experimental measurement is 0.4 eV.[3] So BiCuTeO can be regarded as a narrow-bandgap semiconductor. Accordingly, the temperature-dependent Fermi energy E_F can be calculated by

$$N_C\, e^{-\beta(E_C-E_F)} + N_A\left[1 - \frac{1}{e^{-\beta(E_F-E_A)}+1}\right] = N_V\, e^{-\beta(E_F-E_V)} \quad (2)$$

$$N_C(T) = 2.5\left(\frac{m_e}{m_0}\right)^{\frac{3}{2}}\left(\frac{T}{300\ \mathrm{K}}\right)^{\frac{3}{2}} 10^{19}\ \mathrm{cm}^{-3} \quad (3)$$

$$N_V(T) = 2.5\left(\frac{m_v}{m_0}\right)^{\frac{3}{2}}\left(\frac{T}{300\ \mathrm{K}}\right)^{\frac{3}{2}} 10^{19}\ \mathrm{cm}^{-3} \quad (4)$$

In the eqn (3) and (4), N_C is the conduction band electron number, and N_V is the valence band electron number, m_e is the effective mass of the conduction band electrons, m_v is the effective mass of the valence band electrons, and m_0 is the electron static mass, respectively.

In the formula (2), (3) and (4), N_C is the conduction band electron number, and N_V is the valence band electron number. E_A is the impurity level provided by Cu defects, m_e is the effective mass of the conduction band electrons, m_v is the effective mass of the valence band electrons, and m_0 is the electron static mass. Set $E_V = 0$, $E_A = 1.73 \times 10^{-4}$ eV (2 K), $E_C = 0.5$ eV, $m_e = m_0$, $m_v = 5m_0$. Based on the formulas from (2) to (4), one can acquire the temperature dependent E_F which is drawn in Fig. 4. When T rises, E_F gets closer and closer to the conduction band, meaning that more electrons will hop through the thermal excitation to the conduction band to participate in the transport, matching the results of the two-band model fitting shown in Fig. 3(d).

3.3 Magnetization curve and discussion

Magnetization–temperature (M–T) curve of zero-field cooling (ZFC) and field-cooled (FC) of BiCuTeO are displayed in Fig. 5(a). The little feature observed in M–T curve under ZFC at temperature around 120 K, the absence of this feature from FC curve is typical sign of a short-range (spin glass-like) static

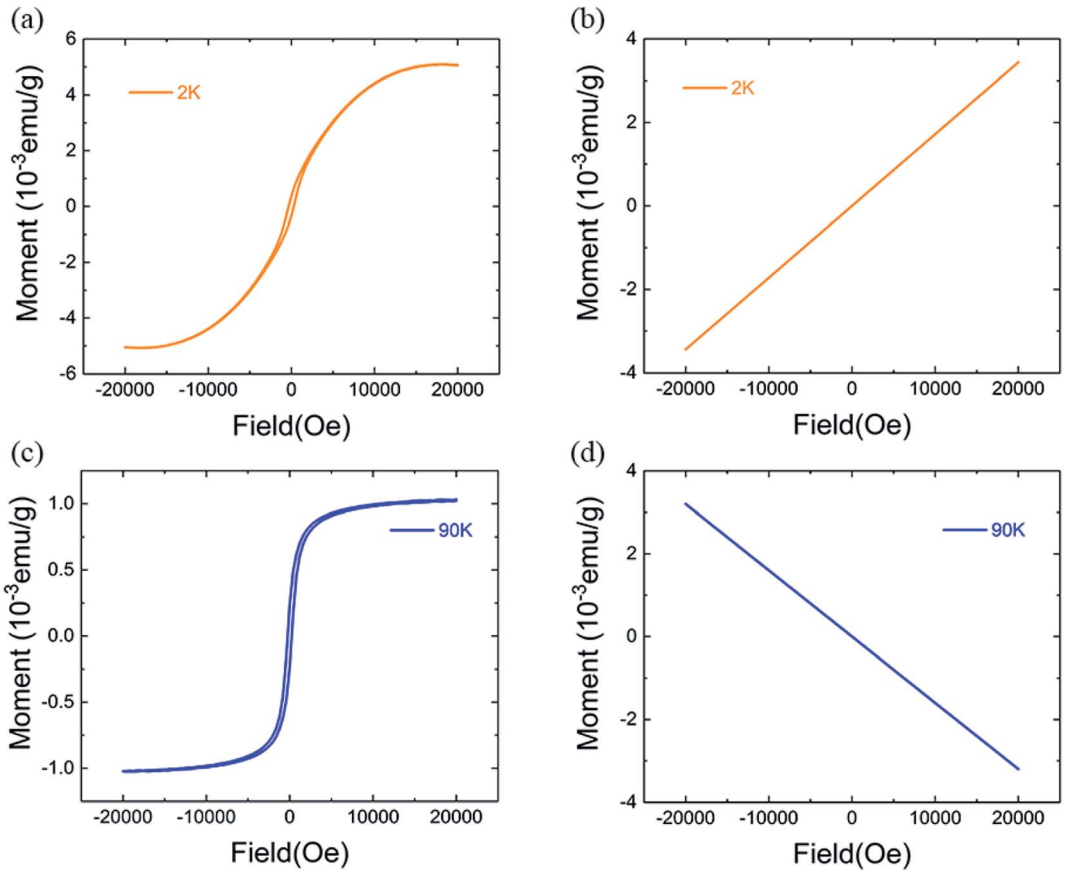

Fig. 6 (a) The detached magnetic hysteresis of BiCuTeO at 2 K. (b) The paramagnetic background of sample at 2 K. (c) The ferromagnetic-like hysteresis of BiCuTeO at 90 K. (d) The diamagnetic background induced by the competition of two types of carriers.

magnetic correlation.[28,29] It should be mentioned that the *M–T* curve measured under ZFC condition has a kink feature at 120 K that is quite different from Néel temperature (~210 K) in antiferromagnetic CuO,[30] which may be an evidence of free-of CuO impurity phase. In the low temperature region, the sample exhibits net moments, which is contributed by a small amount of variable-valent Cu^{2+} ions. The ZFC curve has a turn at around 120 K, which corresponds to the dominant carriers transition observed in the Hall test. Magnetization–magnetic field curves in Fig. 5(b) and (c) show typical signals of the short-range magnetism of the test samples at 2 K, 5 K and 10 K, the loops are closed at around 4000 Oe. When the temperature rises (>10 K), the short-range magnetic correlation is influenced by the thermal fluctuation, the loop narrows further as the temperature increases. Besides, the *M vs. H* curves in Fig. 5(b) do not show signs of saturation, which can also be due to the short-range magnetic correlations.[29] Quantificational, the magnetic hysteresis of BiCuTeO at 2 K can be divided into two parts, the one is hysteresis induced by the short-range magnetic correlation (see Fig. 6(a)), and the other is paramagnetic background (see Fig. 6(b)). Another example is the magnetic hysteresis of sample at 90 K which were also broken up into portions. Specifically, the actual ferromagnetic signal is depicted in Fig. 6(c) and the diamagnetic background (shown in Fig. 6(d)) induced by the competition of electron carriers and hole carriers.

Finally, we'd like to compare the physical property difference of BiCuTeO between this letter and our previous paper.[25] In our previous paper,[25] we observed electrical carriers being holes, and linear magnetic-field-dependent Hall-resistivity, and paramagnetic property. But here we reported the non-linear magnetic-field-dependent Hall-resistivity and short-range magnetism. We believe these differences coming from: BiCuTeO samples characterized in this work have Cu^{2+} ions, while samples reported in our previous paper are mainly Bi-deficient. We wish our work excites further work on BiCuTeO with Cu mixed-valence, maybe there is superconductivity in BiCuXO (X = S, Se and Te) compounds with Cu–Te tetrahedrons, rather than cuprates containing Cu–O squares.

4. Summary

In conclusion, bulk BiCuTeO materials were prepared and subjected to multiple transport and magnetic characterizations. The XRD, EDX and XPS measurements reveal that the sample has a small amount of Cu defects (mixed-valence Cu). This defect makes BiCuTeO show a metal type behavior, and an unsaturated magnetoresistance (MR) about 8% at 2 K with 9 T field and nonlinear Hall resistivities caused by the coexistence of both electron and hole. Using two-band model, the temperature-dependent concentration and mobility of electron and hole were revealed. With the temperature decreased, the dominant carriers changed from electrons to holes. At the turn point (~110 K), the mobility of the sample is also relatively high of about 8.6 $cm^2\ V^{-1}\ S^{-1}$, and the number of electron–holes is quite close. Magnetic measurements show that the BiCuTeO sample has the short-range magnetism at low temperatures, which comes from a small amount of Cu^{2+} ions. This work provides experimental reference for exploring more unique physical properties in BiCuSO, BiCuSeO and BiCuTeO compounds.

Conflicts of interest

The authors declare no competing financial interest.

Acknowledgements

We'd like to acknowledge the financial support from the State Key Program for Basic Research of China (973 Program) (2015CB659400), the National Natural Science Foundation of China (11574131, 51872134, 51890860, 11890702 and 51902152), the Natural Science Foundation of Jiangsu Province, China (BK20171343), the Foundation for Innovative Research Groups of the National Natural Science Foundation of China (51721001), the National Key R&D Program of China (2016YFA0201104). Y.-Y. Lv acknowledges the financial support from Innovation Program for the Talents of China Postdoctoral Science Foundation (BX20180137) and support from China Postdoctoral Science Foundation (2019M650105).

References

1 A. A. Kordyuk, *Low Temp. Phys.*, 2012, **38**, 888.
2 H. Hosono, A. Yamamoto, H. Hiramatsu and Y. Ma, 2017, arXiv: 1710.08574v1.
3 H. Hiramatsu, H. Yanagi, T. Kamiya, K. Ueda, M. Hirano and H. Hosono, *Chem. Mater.*, 2008, **20**, 326–334.
4 I. Pallecchi, F. Caglieris and M. Putti, *Supercond. Sci. Technol.*, 2016, **29**, 073002.
5 Y. Kamihara, T. Watanabe, M. Hirano and H. Hosono, *J. Am. Chem. Soc.*, 2008, **130**(11), 3296–3297.
6 X. H. Chen, T. Wu, G. Wu, R. H. Liu, H. Chen and D. F. Fang, *Nature*, 2008, **453**, 761–762.
7 Z.-A. Ren, G.-C. Che, X.-L. Dong, J. Yang, W. Lu, W. Yi, X.-L. Shen, Z.-C. Li, L.-L. Sun, F. Zhou and Z.-X. Zhao, *Europhys. Lett.*, 2008, **83**, 17002.
8 G. F. Chen, Z. Li, D. Wu, G. Li, W. Z. Hu, J. Dong, P. Zheng, J. L. Luo and N. L. Wang, *Phys. Rev. Lett.*, 2008, **100**, 247002.
9 K. Ueda, S. Inoue, S. Hirose, H. Kawazoe and H. Hosono, *Appl. Phys. Lett.*, 2000, **77**, 2701.
10 K. Ueda, K. Takafuji, H. Hiramatsu, H. Ohta, T. Kamiya, M. Hirano and H. Hosono, *Chem. Mater.*, 2003, **15**(19), 3692–3695.
11 L. D. Zhao, D. Berardan, Y. L. Pei, C. Byl, L. Pinsard-Gaudart and N. Dragoe, *Appl. Phys. Lett.*, 2010, **97**, 092118.
12 G. Tan, L.-D. Zhao and M. G. Kanatzidis, *Chem. Rev.*, 2016, **116**(19), 12123–12149.
13 X. Zhang, C. Chang, Y. Zhou and L. D. Zhao, *Materials*, 2017, **10**(2), 198.
14 J. L. Lan, Y. C. Liu, B. Zhan, Y.-H. Lin, B. P. Zhang, X. Yuan, W. Q. Zhang, W. Xu and C. W. Nan, *Adv. Mater.*, 2013, **25**, 5086–5090.

15 Y.-L. Pei, H. J. Wu, D. Wu, F. S. Zheng and J. Q. He, *J. Am. Chem. Soc.*, 2014, **136**, 13902–13908.
16 J. H. Sui, J. Li, J. Q. He, Y.-L. Pei, D. Berardan, H. J. Wu, N. Dragoe, W. Cai and L.-D. Zhao, *Energy Environ. Sci.*, 2013, **6**, 2916–2920.
17 Y. Liu, L. D. Zhao, Y. C. Zhu, Y. C. Liu, F. Li, M. J. Yu, D. B. Liu, W. Xu, Y. H. Lin and C. W. Nan, *Adv. Energy Mater.*, 2016, **6**, 1502423.
18 L. Zhou, C. Xiao, S. Fan, Y. Deng, W. Zhang, B. Ye and Y. Xie, *J. Am. Chem. Soc.*, 2015, **137**(20), 6587–6593.
19 T.-L. Chou, G. C. Tewari, T.-S. Chan, Y.-Y. Hsu, H. Yamauchi and M. Karppinen, *Solid State Commun.*, 2015, **206**, 12–16.
20 S. K. Karna, C.-H. Hung, C.-M. Wu, C.-W. Wang, W.-H. Li, R. Sankar, F. C. Chou and M. Avdeev, *Dalton Trans.*, 2013, **42**, 15581.
21 S. K. Karna, C.-W. Wang, C.-M. Wu, C.-K. Hsu, D. Hsu, C.-J. Wang, W.-H. Li, R. Sankar and F.-C. Chou, *J. Phys.: Condens. Matter*, 2012, **24**, 266004.
22 I. R. Shein and A. L. Ivanovskii, *Solid State Commun.*, 2010, **150**, 640–643.
23 A. Ubaldini, E. Giannini, C. Senatore and D. van der Marel, *Physica C*, 2010, **470**, S356–S357.
24 A. Pal, H. Kishan and V. P. S. Awana, *J. Supercond. Novel Magn.*, 2010, **23**, 301–304.
25 S.-S. Chen, Y.-C. Luo, Y.-Y. Zhang, S.-T. Dong, Y.-Y. Lv, Y.-S. Cui, S.-H. Yao, J. Zhou and Y. B. Chen, *J. Appl. Phys.*, 2019, **126**, 055108.
26 B. Amal, A. Curutchet, Z. Ahmed, H. A. Ahsaine, P. Sautet, K. Takanabe and T. Le Bahers, *Chem. Mater.*, 2017, **29**(20), 8679–8689.
27 Y. K. Luo, H. Li, Y. M. Dai, H. Miao, Y. G. Shi, H. Ding, A. J. Taylor, D. A. Yarotski, R. P. Prasankumar and J. D. Thompson, *Appl. Phys. Lett.*, 2015, **107**, 182411.
28 E. M. Kenney, C. U. Segre, W. Lafargue-Dit-Hauret, O. I. Lebedev, M. Abramchuk, B. Adam, S. P. Cottrell, G. Simutis, F. Bahrami, N. E. Mordvinova, G. Fabbris, J. L. McChesney, D. Haskel, X. Rocquefelte, M. J. Graf and F. Tafti, *Phys. Rev. B*, 2019, **100**, 094418.
29 C. A. Cardoso, F. M. Araujo-Moreira, V. P. S. Awana, E. Takayama-Muromachi, O. F. de Lima, H. Yamauchi and M. Karppinen, *Phys. Rev. B: Condens. Matter Mater. Phys.*, 2003, **67**, 020407.
30 D. D. Lawrie, J. P. Franck and C. T. Lin, *Physica C*, 1998, **297**, 59–63.